Journal of
Intelligent Material
Systems and Structures

Original Article

Journal of Intelligent Material Systems and Structures
24(16) 1969–1984

DOI: 10.1177/1045389X13488249
jim.sagepub.com
SAGE

Three-dimensional vertical cracks in magnetoelectroelastic media via the extended displacement discontinuity boundary integral equation method

MingHao Zhao[1], ZhengHua Guo[1], CuiYing Fan[1], RongLi Zhang[1] and Ernie Pan[1,2]

Abstract

In this article, the extended displacement discontinuity method is extended to study the fracture problem in a three-dimensional transversely isotropic magnetoelectroelastic medium with a planar crack vertical to the plane of isotropy. Considering the electric and magnetic fields in the crack cavity, and using the Somigliana identity along with the displacement discontinuity Green's functions, the hyper-singular boundary integral equations for the unknown displacement discontinuities across the crack face are derived. The singularity features along the crack fronts are analyzed, and the extended field intensity factors are expressed in terms of the extended displacement discontinuities on the crack face. Numerical examples on the field intensity factors are finally calculated for a vertical square crack using the exact closed-form Green's functions due to constant displacement discontinuities over a rectangular crack element, and some interesting features are observed, which are different from the case where the crack is located in the plane of isotropy. The influence of the electric and magnetic boundary conditions along the crack face on the field intensity factors is further studied.

Keywords

Magnetoelectroelastic medium, displacement discontinuity solution, boundary integral equation method, vertical crack, field intensity factor

Introduction

Due to the multifield coupling among the mechanical, magnetic, and electric fields, magnetoelectroelastic (MEE) materials are being widely used as smart structures in many high-tech fields (Dinzart and Sabar, 2012; Huang et al., 2009; Lee et al., 2005; Li and Dunn, 1998). In applications, however, unavoidable defects (e.g. cracks) in these materials exist, which requires us to analyze the fracture behavior of cracks in MEE media (Chen, 2009; Feng et al., 2010; Gao and Noda, 2004; Li et al., 2009; Rojas-Díaz et al., 2010; Wang, 2012; Zhao et al., 2010; Zhong, 2009; Gao et al., 2003a, 2003b; Jiang and Pan, 2004; Liu et al., 2001).

For some MEE materials, when the applied electric/magnetic field is removed, the electric/magnetic dipoles remain inside the material. Thus, the electric/magnetic polarization could play an important role in the material properties and fracture mechanics features. The influence of crack orientation on fractures in two-dimensional (2D) MEE solids was analyzed by Sih and Song (2003), Sih et al. (2003), and Spyropoulos et al. (2003). These results showed that both the crack orientation and electric/magnetic poling direction could significantly affect the field intensity factors and then the crack growth. As for the corresponding three-dimensional (3D) case, most previous studies were for the simple situation where the cracks are located in the

[1]School of Mechanical Engineering, Zhengzhou University, Zhengzhou, China
[2]Department of Civil Engineering, College of Engineering, University of Akron, Akron, OH, USA

Corresponding author:
Ernie Pan, Department of Civil Engineering, College of Engineering, University of Akron, Akron, OH 44325, USA.
Email: pan2@uakron.edu

plane of isotropy (Sladek et al., 2008; Zhao et al., 2007a, 2007b). In general, however, a crack could be oriented arbitrarily in the 3D space. Therefore, as the first extension, we consider, in this article, the more complicated case where the crack is located in a vertical plane of the 3D transversely isotropic MEE media or with its normal parallel to the plane of isotropy.

Various numerical methods can be applied to fracture analysis, including the displacement discontinuity boundary integral equation method (Crouch, 1976) proposed for elastic solids. It can be extended to MEE media (Pan and Yuan, 2000; Rangelov et al., 2011; Rojas-Díaz et al., 2012; Wünsche et al., 2012; Zhao et al., 1994, 2007a, 2007b). This method is very convenient in handling stress concentration and singularity, although it requires the corresponding Green's functions due to the concentrated extended displacement discontinuity.

Thus, in this article, using the extended displacement discontinuity fundamental solution for a vertical crack in a 3D MEE space, we establish the corresponding displacement discontinuity boundary integral equations under different electric–magnetic boundary conditions. We then apply our novel boundary integral equations to a vertical square crack in a 3D transversely isotropic MEE medium to calculate the extended field intensity factors along the crack fronts. This article is organized as follows. In section "Basic equations," we present the basic equations for a 3D transversely isotropic MEE medium and also present the different boundary conditions. In section "Boundary integral equations for vertical planar cracks in 3D MEE media," we derive the extended displacement discontinuity boundary integral equations using the point-discontinuity Green's functions and analyze the singularity behavior and the field intensity factors along the crack fronts. The corresponding boundary element method based on the extended displacement discontinuity is presented in section "Extended displacement discontinuity boundary element method" using the exact closed-form displacement discontinuity Green's function over a rectangular element. Numerical results for a vertical square crack are given in section "Numerical results and discussion," and conclusions are drawn in section "Conclusion."

Basic equations

Constitutive equations

For a 3D transversely isotropic MEE medium in the Cartesian coordinates $(x, y, z) \equiv (x_1, x_2, x_3)$ with its poling direction along the z-axis, the extended equilibrium equations in the absence of the mechanical, electric, and magnetic sources as well as the constitutive equations can be expressed as (Soh and Liu, 2005)

$$\sigma_{ij,i} = 0, \quad D_{i,i} = 0, \quad B_{i,i} = 0 \tag{1a}$$

$$\begin{aligned} \sigma_{ij} &= C_{ijkl}\, uk_l + e_{lij}\varphi_{,l} + q_{lij}\psi_{,l} \\ D_i &= e_{ikl}\, uk_l - \varepsilon_{il}\varphi_{,l} - \alpha_{il}\psi_{,l} \\ B_i &= q_{ikl}\, uk_l - \alpha_{il}\varphi_{,l} - \mu_{il}\psi_{,l} \end{aligned} \tag{1b}$$

where σ_{ij}, D_i, and B_i denote the stresses, electric displacements, and magnetic inductions, respectively; u_k, ϕ, and ψ denote the elastic displacements, electric potential, and magnetic potential, respectively; C_{ijkl} $(\equiv c_{mn})$, e_{lij} $(\equiv e_{lm})$, and ε_{il} denote the elastic, piezoelectric, and electric permittivity coefficients, respectively; q_{lij} $(\equiv q_{lm})$, α_{il}, and μ_{il} denote the piezomagnetic, magnetoelectric, and magnetic permeability coefficients, respectively. Furthermore, in equation (1), the subscript ",i" denotes the partial derivative with respect to the coordinate variable x_i, and a repeated index, for example, i, implies summation from 1 to 3.

For convenience, equation (1) can be equivalently expressed in a compact form as

$$\sigma_{iJ,i} = 0 \tag{2a}$$

$$\sigma_{iJ} = C_{iJKl} u_{K,l} \tag{2b}$$

where the capital subscripts J and K vary from 1 to 5, and the lowercase indices i and l range from 1 to 3. While the generalized stresses are defined as $\sigma_{iJ}|_{J=1-5} = (\sigma_{ix}, \sigma_{iy}, \sigma_{iz}, D_i, B_i)$, the generalized displacements as $u_K|_{K=1-5} = (u_1, u_2, u_3, u_4, u_5) \equiv (u_x, u_y, u_z, \phi, \psi)$. The extended elastic stiffness coefficients are defined as

$$C_{iJKl} = \begin{cases} C_{ijkl} & J,K = j,k = 1,2,3 \\ e_{lij}/e_{ikl} & J = j = 1,2,3, K = 4/J = 4, K = k = 1,2,3 \\ q_{lij}/q_{ikl} & J = j = 1,2,3, K = 5/J = 5, K = k = 1,2,3 \\ -\varepsilon_{il} & J,K = 4 \\ -\alpha_{il}/-\alpha_{li} & J = 4; K = 5/J = 5; K = 4 \\ -\mu_{il} & J,K = 5 \end{cases} \tag{3}$$

In the subscript notation, ij or kl is replaced by m or n, where values of i, j, k, and l in equation (3) take 1, 2, and 3 and m, n vary from 1 to 6, as shown in Table 1 (Nye, 1957; Soh and Liu, 2005).

Table 1. Correspondence between subscripts ij (1–3) and subscript m (1–6).

ij	m
11	1
22	2
33	3
23 or 32	4
13 or 31	5
12 or 21	6

Electric and magnetic boundary conditions

Considering a crack with its normal along x-direction, the possible electric displacement D_x^c and magnetic induction B_x^c in the crack cavity can be expressed as

$$\begin{aligned} D_x(0^+, y, z) &= D_x(0^-, y, z) = D_x^c(0, y, z) \\ B_x(0^+, y, z) &= B_x(0^-, y, z) = B_x^c(0, y, z) \end{aligned} \tag{4a}$$

The differences of the elastic displacement, electric potential, and magnetic potential on the two crack surfaces (S^+ and S^-), which are also called the extended displacement discontinuities, are expressed as follows

$$(\Delta u_x, \Delta u_y, \Delta u_z, \Delta\varphi, \Delta\psi) = \Delta u_I = u_I(S^+) - u_I(S^-) \tag{4b}$$

Based on these quantities, five kinds of electric and magnetic boundary conditions on the crack face can be studied (Zhao et al., 2007b).

(1) Electrically and magnetically impermeable condition

$$D_x^c(0, y, z) = 0, \qquad B_x^c(0, y, z) = 0 \tag{5}$$

(2) Electrically and magnetically permeable condition

$$\Delta\varphi(0, y, z) = 0, \qquad \Delta\psi(0, y, z) = 0 \tag{6}$$

(3) Electrically impermeable and magnetically permeable condition

$$D_x^c(0, y, z) = 0, \qquad \Delta\psi(0, y, z) = 0 \tag{7}$$

(4) Electrically permeable and magnetically impermeable condition

$$\Delta\varphi(0, y, z) = 0, \qquad B_x^c(0, y, z) = 0 \tag{8}$$

(5) Crack opening model (or the electrically and magnetically semi-permeable boundary condition)

$$\begin{aligned} D_x^c(0, y, z) &= -\varepsilon^c \frac{\Delta\varphi(0, y, z)}{\Delta u_x(0, y, z)}, \\ B_x^c(0, y, z) &= -\mu^c \frac{\Delta\psi(0, y, z)}{\Delta u_x(0, y, z)} \end{aligned} \tag{9}$$

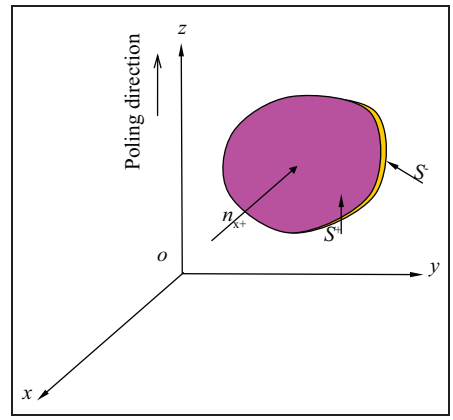

Figure 1. A transversely isotropic magnetoelectroelastic medium with an arbitrarily shaped crack in the *oyz* plane.

Boundary integral equations for vertical planar cracks in 3D MEE media

Boundary integral equations

For a transversely isotropic MEE infinite medium, we set up the Cartesian coordinate system $oxyz$ (or $x_1x_2x_3$) with the oxy plane parallel to the plane of isotropy and the poling direction along the z-axis. We assume that there is an arbitrarily shaped vertical crack S located in the oyz plane (Figure 1). The two surfaces of the crack S are denoted by S^+ and S^-, respectively, with the outward normal vectors of S^+ and S^- being given by $n_{i+} = (-1, 0, 0)$ and $n_{i-} = (1, 0, 0)$, respectively (Figure 1).

The applied extended tractions on the crack faces are assumed to satisfy

$$p_I|_{S^+} = -p_I|_{S^-} \tag{10}$$

in which the extended tractions are defined as $p_I|_{I=1-5} = (p_1, p_2, p_3, p_4, p_5) \equiv (p_x, p_y, p_z, \overline{D}, \overline{B})$, with p_x, p_y, and p_z being the elastic tractions on the crack face along x-, y-, and z-directions, respectively, and $\overline{D}$ and $\overline{B}$ being, respectively, the given electric and magnetic loads on the crack face in x-direction.

Following the boundary integral equation approach (Zhao et al., 2007b, 2012) and making use of the Somigliana identity and the Green's functions for the extended point-displacement discontinuity given in Appendix 1, we obtain the following boundary integral equations for the extended displacement discontinuity on a planar vertical crack of arbitrary shape under the described crack surface conditions (5) to (10) for the 3D MEE medium

$$\int_{S^+}\left\{4L_{11}^5\left[(\eta-y)^2\left(\frac{2}{r_5^2\tilde{r}_5^3}+\frac{1}{r_5^3\tilde{r}_5^2}\right)-\frac{1}{r_5\tilde{r}_5^2}\right]+\sum_{i=1}^{4}\left(6L_{12}^i+2L_{13}^i\right)\frac{1}{r_i\tilde{r}_i^2}\right.$$

$$-\sum_{i=1}^{4}2L_{13}^i(\eta-y)^2\left(\frac{2}{r_i^2\tilde{r}_i^3}+\frac{1}{r_i^3\tilde{r}_i^2}\right)-\sum_{i=1}^{4}\left(L_{14}^i+L_{15}^i+2L_{16}^i+L_{17}^i\right)\frac{1}{r_i^3}+\sum_{i=1}^{4}3L_{15}^i\frac{(\eta-y)^2}{r_i^5} \tag{11a}$$

$$\left.+\sum_{i=1}^{4}3L_{17}^i\frac{(\varsigma_i-z_i)^2}{r_i^5}\right\}\Delta u_x\mathrm{d}S(\eta,\varsigma)=-p_x(y,z)$$

$$\int_{S^+}\left\{\left[3L_{11}^5\frac{(\eta-y)^2}{r_5^5}-2L_{11}^5\frac{1}{r_5^3}+4\sum_{i=1}^{5}L_{11}^i\left(\frac{1}{r_i\tilde{r}_i^2}-(\eta-y)^2\left(\frac{2}{r_i^2\tilde{r}_i^3}+\frac{1}{r_i^3\tilde{r}_i^2}\right)\right)\right]\Delta u_y\right.$$

$$+\left(\frac{6(\eta-y)}{r_5^2\tilde{r}_5^2}-(\eta-y)^3\left(\frac{3}{r_5^5\tilde{r}_5}+\frac{3}{r_5^4\tilde{r}_5^2}+\frac{4}{r_5^3\tilde{r}_5^3}\right)\right)\left(L_{31}^5\Delta u_z+L_{32}^5\Delta\varphi+L_{33}^5\Delta\psi\right) \tag{11b}$$

$$\left.-\sum_{i=1}^{4}2(\eta-y)\left(\frac{1}{r_i^2\tilde{r}_i^2}+\frac{1}{r_i^3\tilde{r}_i}\right)\left(L_{34}^i\Delta u_z+L_{35}^i\Delta\varphi+L_{36}^i\Delta\psi\right)\right\}\mathrm{d}S(\eta,\varsigma)=-p_y(y,z)$$

$$\int_{S^+}\left\{\left[\left(2(\eta-y)\left(\frac{1}{r_5^2\tilde{r}_5^2}+\frac{1}{r_5^3\tilde{r}_5}\right)-(\eta-y)^3\left(\frac{2}{r_5^3\tilde{r}_5^3}+\frac{3}{r_5^4\tilde{r}_5^2}+\frac{3}{r_5^5\tilde{r}_5}\right)\right)L_{21}^5\right.\right.$$

$$\left.-\sum_{i=1}^{4}2(\eta-y)\left(\frac{1}{r_i^2\tilde{r}_i^2}+\frac{1}{r_i^3\tilde{r}_i}\right)L_{21}^i\right]\Delta u_y+\left[\frac{1}{r_5^3}-3\frac{(\eta-y)^2}{r_5^5}\right]\left(L_{41}^5\Delta u_z+L_{61}^5\Delta\varphi+L_{81}^5\Delta\psi\right) \tag{11c}$$

$$\left.-\sum_{i=1}^{4}\frac{1}{r_i^3}\left(L_{51}^i\Delta u_z+L_{71}^i\Delta\varphi+L_{91}^i\Delta\psi\right)\right\}\mathrm{d}S(\eta,\varsigma)=-p_z(y,z)$$

$$\int_{S^+}\left\{\left[\left(2(\eta-y)\left(\frac{1}{r_5^2\tilde{r}_5^2}+\frac{1}{r_5^3\tilde{r}_5}\right)-(\eta-y)^3\left(\frac{2}{r_5^3\tilde{r}_5^3}+\frac{3}{r_5^4\tilde{r}_5^2}+\frac{3}{r_5^5\tilde{r}_5}\right)\right)L_{22}^5\right.\right.$$

$$\left.-\sum_{i=1}^{4}2(\eta-y)\left(\frac{1}{r_i^2\tilde{r}_i^2}+\frac{1}{r_i^3\tilde{r}_i}\right)L_{22}^i\right]\Delta u_y+\left[\frac{1}{r_5^3}-3\frac{(\eta-y)^2}{r_5^5}\right]\left(L_{42}^5\Delta u_z+L_{62}^5\Delta\varphi+L_{82}^5\Delta\psi\right) \tag{11d}$$

$$\left.-\sum_{i=1}^{4}\frac{1}{r_i^3}\left(L_{52}^i\Delta u_z+L_{72}^i\Delta\varphi+L_{92}^i\Delta\psi\right)\right\}\mathrm{d}S(\eta,\varsigma)=-\overline{D}(y,z)+D_x^c$$

$$\int_{S^+}\left\{\left[\left(2(\eta-y)\left(\frac{1}{r_5^2\tilde{r}_5^2}+\frac{1}{r_5^3\tilde{r}_5}\right)-(\eta-y)^3\left(\frac{2}{r_5^3\tilde{r}_5^3}+\frac{3}{r_5^4\tilde{r}_5^2}+\frac{3}{r_5^5\tilde{r}_5}\right)\right)L_{23}^5\right.\right.$$

$$\left.-\sum_{i=1}^{4}2(\eta-y)\left(\frac{1}{r_i^2\tilde{r}_i^2}+\frac{1}{r_i^3\tilde{r}_i}\right)L_{23}^i\right]\Delta u_y+\left[\frac{1}{r_5^3}-3\frac{(\eta-y)^2}{r_5^5}\right]\left(L_{43}^5\Delta u_z+L_{63}^5\Delta\varphi+L_{83}^5\Delta\psi\right) \tag{11e}$$

$$\left.-\sum_{i=1}^{4}\frac{1}{r_i^3}\left(L_{53}^i\Delta u_z+L_{73}^i\Delta\varphi+L_{93}^i\Delta\psi\right)\right\}\mathrm{d}S(\eta,\varsigma)=-\overline{B}(y,z)+B_x^c$$

The material-related coefficients L^i_{kl} in equation (11) are given as follows

$$
\begin{aligned}
&L^i_{11} = T_5 c_{66} c_{66},\ L^i_{12} = T_i c_{66} c_{11},\ L^i_{13} = T_i c_{66} c_{12} \\
&L^i_{14} = T_i \xi_i c_{11},\ \ L^i_{15} = T_i \xi_i c_{12},\ \ L^5_{6i} = T_5 e_{15} \omega_{5i} s_5 \\
&L^i_{16} = (A_i c_{13} - N_i e_{31} - C_i q_{31}) c_{66} s_i \\
&L^i_{17} = (A_i c_{13} - N_i e_{31} - C_i q_{31}) \xi_i s_i \\
&L^i_{2j} = T_i \omega_{ij} c_{66},\ L^5_{31} = T_5 c_{66} c_{44} s_5 \\
&L^i_{34} = c_{66}(c_{44} T_i s_i + c_{44} A_i - e_{15} N_i - q_{15} C_i) \\
&L^5_{4i} = T_5 c_{44} \omega_{5i} s_5,\ L^5_{32} = T_5 c_{66} e_{15} s_5 \\
&L^i_{5j} = \omega_{ij}(c_{44} T_i s_i + c_{44} A_i - e_{15} N_i - q_{15} C_i) \\
&L^i_{35} = c_{66}(e_{15} T_i s_i + e_{15} A_i + \varepsilon_{11} N_i + \alpha_{11} C_i) \\
&L^i_{7j} = \omega_{ij}(e_{15} T_i s_i + e_{15} A_i + \varepsilon_{11} N_i + \alpha_{11} C_i) \\
&L^5_{33} = T_5 c_{66} q_{15} s_5,\ L^5_{8i} = T_5 q_{15} \omega_{5i} s_5 \\
&L^i_{36} = c_{66}(q_{15} T_i s_i + q_{15} A_i + \alpha_{11} N_i + \mu_{11} C_i) \\
&L^i_{9j} = \omega_{ij}(q_{15} T_i s_i + q_{15} A_i + \alpha_{11} N_i + \mu_{11} C_i)
\end{aligned}
\tag{12a}
$$

and

$$
\begin{aligned}
r_i &= \sqrt{(\eta - y)^2 + (\varsigma_i - z_i)^2} \\
\tilde{r}_i &= \sqrt{(\eta - y)^2 + (\varsigma_i - z_i)^2} + (\varsigma_i - z_i)
\end{aligned}
\tag{12b}
$$

with ω_{ij}, ξ_i, A_i, N_i, C_i, and T_i being related to the extended elastic coefficients C_{iJKl} (Soh and Liu, 2005; Zhao et al., 2007a, 2007b). Because D_i and B_i are used to denote the electric displacement and magnetic induction in this article, the material constants D_i and B_i in Zhao et al. (2007a, 2007b) are replaced by T_i and N_i, respectively.

Equation (11) is a set of boundary integral equations of hyper-singularity and possesses the following important feature. Equation (11a) contains only the elastic displacement discontinuity Δu_x and the elastic traction p_x, while the other four extended displacement discontinuities Δu_y, Δu_z, $\Delta\varphi$, and $\Delta\psi$ are coupled together in equations (11b) to (11e). In other words, the loading and displacement discontinuities in the x-direction are purely elastic and are decoupled from other elastic and magnetic/electric components.

This interesting feature is completely different from the feature when a crack is located in the isotropic plane (Zhao et al., 2007b), where the displacement discontinuities Δu_x and Δu_y on the crack faces are coupled and the displacement discontinuity Δu_z, electric potential discontinuity $\Delta\varphi$, and magnetic potential discontinuity $\Delta\psi$ are also coupled.

Singularity behavior at the crack front and field intensity factors

Following the same approach as in Zhao et al. (2007b, 2012), one can easily approve that the extended displacements near the crack tip have the same asymptotic order of $r^{-1/2}$ as in the classical fracture mechanics of conventional elastic materials. Therefore, we can define the intensity factors as (e.g. for the crack tip on the z-axis)

$$
\begin{aligned}
K_{\mathrm{I}} &= \lim_{\rho\to 0} \sqrt{2\pi\rho}\,\sigma_{xx}(0,0,-\rho) \\
K_{\mathrm{II}} &= \lim_{\rho\to 0} \sqrt{2\pi\rho}\,\sigma_{xz}(0,0,-\rho) \\
K_{\mathrm{III}} &= \lim_{\rho\to 0} \sqrt{2\pi\rho}\,\sigma_{xy}(0,0,-\rho) \\
K_D &= \lim_{\rho\to 0} \sqrt{2\pi\rho}\,D_x(0,0,-\rho) \\
K_B &= \lim_{\rho\to 0} \sqrt{2\pi\rho}\,B_x(0,0,-\rho)
\end{aligned}
\tag{13}
$$

in which ρ denotes the distance from the crack tip.

According to equations (11) and (13), at the crack tips (i.e. at the lowest and highest points) of the vertical crack front, the extended field intensity factor can be expressed in terms of the extended displacement discontinuities as (with local $z = 0$ at the crack tip)

$$
\begin{aligned}
K_I &= \sqrt{2\pi}\pi \lim_{z\to 0} k_{11}\Delta u_x/\sqrt{z} \\
K_{II} &= -\sqrt{2\pi}\pi \lim_{z\to 0} \sum_{i=1}^{4} \left[L^i_{51}\Delta u_z + L^i_{71}\Delta\varphi + L^i_{91}\Delta\psi\right] \frac{1}{s_i^2}/\sqrt{z} \\
K_{III} &= \sqrt{2\pi}\pi \lim_{z\to 0} k_{12}\Delta u_y/\sqrt{z} \\
K_D &= -\sqrt{2\pi}\pi \lim_{z\to 0} \sum_{i=1}^{4} \left[L^i_{52}\Delta u_z + L^i_{72}\Delta\varphi + L^i_{92}\Delta\psi\right] \frac{1}{s_i^2}/\sqrt{z} \\
K_B &= -\sqrt{2\pi}\pi \lim_{z\to 0} \sum_{i=1}^{4} \left[L^i_{53}\Delta u_z + L^i_{73}\Delta\varphi + L^i_{93}\Delta\psi\right] \frac{1}{s_i^2}/\sqrt{z}
\end{aligned}
\tag{14a}
$$

where

$$
k_{11} = \sum_{i=1}^{4} \frac{1}{s_i^2}\left(2L^i_{12} - L^i_{14} - 2L^i_{16} + L^i_{17}\right),\ \ k_{12} = \frac{L^5_{11}}{s_5^2}
\tag{14b}
$$

Similarly, the extended field intensity factors at the crack tips (i.e. at the farthest left and farthest right of the crack front, with local $y = 0$ at the crack tip) can be expressed in terms of the extended displacement discontinuities as

$$K_{\mathrm{I}} = \sqrt{2\pi}\pi \lim_{y\to 0} k_{21}\Delta u_x/\sqrt{y}$$

$$K_{\mathrm{II}} = -\sqrt{2\pi}\pi \lim_{y\to 0} \sum_{i=1}^{4} \left[k_{61}\Delta u_y + k_{51}\Delta u_z + k_{31}\Delta\varphi + k_{41}\Delta\psi\right]/\sqrt{y}$$

$$K_{\mathrm{III}} = -\sqrt{2\pi}\pi \lim_{y\to 0} \sum_{i=1}^{4} \left[k_{62}\Delta u_y + k_{52}\Delta u_z + k_{32}\Delta\varphi + k_{42}\Delta\psi\right]/\sqrt{y}$$

$$K_D = -\sqrt{2\pi}\pi \lim_{y\to 0} \sum_{i=1}^{4} \left[k_{63}\Delta u_y + k_{53}\Delta u_z + k_{33}\Delta\varphi + k_{43}\Delta\psi\right]/\sqrt{y}$$

$$K_B = -\sqrt{2\pi}\pi \lim_{y\to 0} \sum_{i=1}^{4} \left[k_{64}\Delta u_y + k_{54}\Delta u_z + k_{34}\Delta\varphi + k_{44}\Delta\psi\right]/\sqrt{y} \tag{15a}$$

where the material-related constants are given as follows

$$k_{21} = \frac{2L_{11}^5}{s_5} + \sum_{i=1}^{4}\left[3L_{12}^i - L_{13}^i - L_{14}^i + L_{15}^i - 2L_{16}^i\right]\frac{1}{s_i}$$

$$k_{31} = \frac{1}{s_5}L_{32}^5 + \sum_{i=1}^{4}\frac{2}{s_i}L_{35}^i,\quad k_{32} = \frac{1}{s_5}L_{61}^5 + \sum_{i=1}^{4}\frac{1}{s_i}L_{71}^i$$

$$k_{33} = \frac{1}{s_5}L_{62}^5 + \sum_{i=1}^{4}\frac{1}{s_i}L_{72}^i,\quad k_{34} = \frac{1}{s_5}L_{63}^5 + \sum_{i=1}^{4}\frac{1}{s_i}L_{73}^i$$

$$k_{41} = \frac{1}{s_5}L_{33}^5 + \sum_{i=1}^{4}\frac{2}{s_i}L_{36}^i,\quad k_{42} = \frac{1}{s_5}L_{81}^5 + \sum_{i=1}^{4}\frac{1}{s_i}L_{91}^i$$

$$k_{43} = \frac{1}{s_5}L_{82}^5 + \sum_{i=1}^{4}\frac{1}{s_i}L_{92}^i,\quad k_{44} = \frac{1}{s_5}L_{83}^5 + \sum_{i=1}^{4}\frac{1}{s_i}L_{93}^i \tag{15b}$$

$$k_{51} = \frac{1}{s_5}L_{31}^5 + \sum_{i=1}^{4}\frac{2}{s_i}L_{34}^i,\quad k_{52} = \frac{1}{s_5}L_{41}^5 + \sum_{i=1}^{4}\frac{1}{s_i}L_{51}^i$$

$$k_{53} = \frac{1}{s_5}L_{42}^5 + \sum_{i=1}^{4}\frac{1}{s_i}L_{52}^i,\quad k_{54} = \frac{1}{s_5}L_{43}^5 + \sum_{i=1}^{4}\frac{1}{s_i}L_{53}^i$$

$$k_{61} = \sum_{i=1}^{5}\frac{2}{s_i}L_{11}^i,\quad k_{62} = \frac{1}{s_5}L_{21}^5 + \sum_{i=1}^{4}\frac{2}{s_i}L_{21}^i$$

$$k_{63} = \frac{1}{s_5}L_{22}^5 + \sum_{i=1}^{4}\frac{2}{s_i}L_{22}^i,\quad k_{64} = \frac{1}{s_5}L_{23}^5 + \sum_{i=1}^{4}\frac{2}{s_i}L_{23}^i \tag{15c}$$

Equations (14) and (15) state that for the vertical crack case, the mode I stress intensity factor K_{I} depends on the normal elastic displacement discontinuity Δu_x only, while the mode II stress intensity factor K_{II}, the electric displacement intensity factor K_D, and the magnetic displacement intensity factor K_B are all coupled together with the elastic displacement discontinuities Δu_y and Δu_z and with the electric ($\Delta\varphi$) and magnetic ($\Delta\psi$) potential discontinuities. As such, the relations between the extended field intensity factors and the extended displacement discontinuities for a vertical crack are remarkably different from those when the crack face is parallel to the isotropic plane of the MEE media (Zhao et al., 2007b).

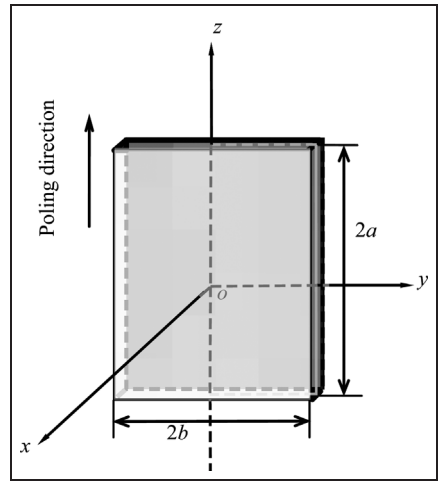

Figure 2. A rectangular crack element in the *oyz* plane with its centroid located at the origin of the coordinate system.

Extended displacement discontinuity boundary element method

If a uniformly distributed extended displacement discontinuities Δu_I are applied on the rectangular element S_e in the *oyz* plane, as shown in Figure 2, the induced extended traction field can be expressed as

$$p_J = \sum_{I=1}^{5} T_{IJ}\Delta u_I, \qquad I, J = 1-5 \tag{16}$$

where T_{IJ} are the special traction Green's functions or the extended fundamental traction solutions induced by the extended displacement discontinuities over a rectangular element. We have derived their exact closed expressions, and the results are given in Appendix 2.

For a given crack, we now divide its entire face into N square elements and denote the geometric centroid of the eth element by (y_e, z_e) and the qth element by (y_q, z_q). Based on the extended fundamental solution and by superposing the contributions from all elements, we can obtain the following extended displacement discontinuity boundary element equations

$$\begin{aligned} &\sum_{e=1}^{N}\sum_{I=1}^{5} T_{IJ}(x_q - x_e,\ y_q - y_e,\ z_q - z_e) \\ &\Delta u_I = p_J(q),\ q = 1, 2, \ldots, N \end{aligned} \tag{17}$$

where $p_J(q)$ are the given boundary values on the crack face.

Thus, for given extended tractions on the crack face, equation (17) can be solved for the extended displacement discontinuities on the crack face. Then, the extended field intensity factors can be calculated using equations (14) and (15).

Numerical results and discussion

As a numerical example, we consider a square crack of side length $2a$ located in the oyz plane of an infinite MEE space ($2b = 2a$ in Figure 2). The MEE space is made of the composite $BaTiO_3$–$CoFe_2O_4$, with $CoFe_2O_4$ as matrix and $BaTiO_3$ as inhomogeneity. The volume fraction of the inhomogeneity is denoted as V_i, and the material coefficients of the individuals are given as follows.

$BaTiO_3$

$$\begin{aligned}
&c_{11} = 166\ \text{GPa}, \quad c_{33} = 162\ \text{GPa}, \quad c_{44} = 43\ \text{GPa},\\
&c_{12} = 77\ \text{GPa}, \quad c_{13} = 78\ \text{GPa} \quad e_{31} = -4.4\ \text{C/m}^2,\\
&e_{33} = 18.6\ \text{C/m}^2, \quad e_{15} = 11.6\ \text{C/m}^2\\
&\varepsilon_{11} = 11.2\times10^{-9}\ \text{C}^2/(\text{N m}^2),\\
&\varepsilon_{33} = 12.6\times10^{-9}\ \text{C}^2/(\text{N m}^2)\\
&\mu_{11} = 5.0\times10^{-6}\ \text{N s}^2/\text{C}^2, \quad \mu_{33} = 10.0\times10^{-6}\ \text{N s}^2/\text{C}^2
\end{aligned} \tag{18}$$

$CoFe_2O_4$

$$\begin{aligned}
&c_{11} = 286\ \text{GPa}, \quad c_{33} = 269.5\ \text{GPa}, \quad c_{44} = 45.3\ \text{GPa},\\
&c_{12} = 173.0\ \text{GPa} \quad c_{13} = 170.5\ \text{GPa}\\
&f_{31} = 580.3\ \text{N/(A m)}, \quad f_{33} = 699.7\ \text{N/(A m)},\\
&f_{15} = 550\ \text{N/(A m)}\\
&\varepsilon_{11} = 0.08\times10^{-9}\ \text{C}^2/(\text{N m}^2),\\
&\varepsilon_{33} = 0.093\times10^{-9}\ \text{C}^2/(\text{N m}^2)\\
&\mu_{11} = 590\times10^{-6}\ \text{N s}^2/\text{C}^2, \quad \mu_{33} = 157\times10^{-6}\ \text{N s}^2/\text{C}^2
\end{aligned} \tag{19}$$

In this article, we assume that $V_i = 0.5$, with the composite material coefficients being determined by the following simple relation

$$\Lambda^c = \Lambda^i V_i + \Lambda^m(1 - V_i) \tag{20}$$

where the superscripts c, i, and m represent composite material, inhomogeneity, and matrix, respectively.

Following our previous comparison study using the finite element software ANSYS (Zhao et al., 2012), we divide the square crack into 25×25 constant elements to ensure that the numerical results presented in this article have a relative error less than 6%.

A square crack under electrically and magnetically impermeable condition

Figure 3 shows the normalized mode I stress intensity factor F_I along the crack front under the electrically and magnetically impermeable condition (equation (5)) with an applied mechanical load p_x on the crack surface (other loads are zero)

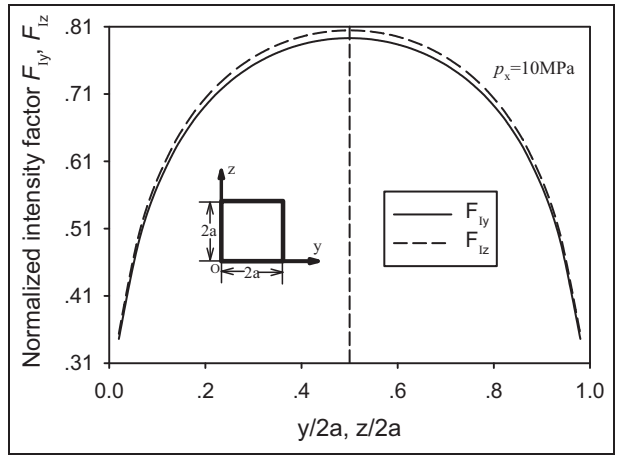

Figure 3. Variation of the normalized mode I stress intensity factors along the crack front parallel to y-axis (F_{Iy}) and z-axis (F_{Iz}) under mechanical load p_x = 10 MPa on the crack surface (other loads on the crack surface are zero).

$$F_I = \frac{K_I}{p_x\sqrt{\pi a}} \tag{21}$$

In Figure 3, the subscripts "z" and "y" denote the crack fronts parallel to the z- and y-axes, respectively. It is observed that a mechanical load in x-direction induces only the mode I stress intensity factor along the crack fronts and that this stress intensity factor is symmetric with respect to the midpoint of the crack front with a maximum value at the midpoint. However, due to the fact that the poling direction is along the z-axis, the stress intensity factor along the crack front parallel to the z-axis (F_{Iz}) is slightly larger than that parallel to the y-axis (F_{Iy}).

Figure 4(a) and (b) shows the normalized extended field intensity factors F_{II}, F_{III}, F_D, and F_B along the crack fronts parallel to the y- and z-axes, respectively. The mechanical shear load on the crack surface is p_z = 10 MPa while other loads are assumed to be zero. Figure 5(a) and (b) shows the plots of the corresponding results when a uniform shear load p_y = 10 MPa is applied on the crack face. The normalized field intensity factors are defined as follows

$$\begin{aligned}
F_{II} &= \frac{K_{II}}{p\sqrt{\pi a}}, \quad F_{III} = \frac{K_{III}}{p\sqrt{\pi a}},\\
F_D &= \frac{K_D}{\chi_1 p\sqrt{\pi a}}, \quad F_B = \frac{K_B}{\chi_2 p\sqrt{\pi a}}
\end{aligned} \tag{22}$$

with p equal to p_z in Figure 4 and p_y in Figure 5. Also, in equation (22), $\chi_1 = \varepsilon_{33}/e_{33}$ and $\chi_2 = \mu_{33}/q_{33}$.

It is pointed out that due to the special orientation of the crack and the mechanical load applied, there is

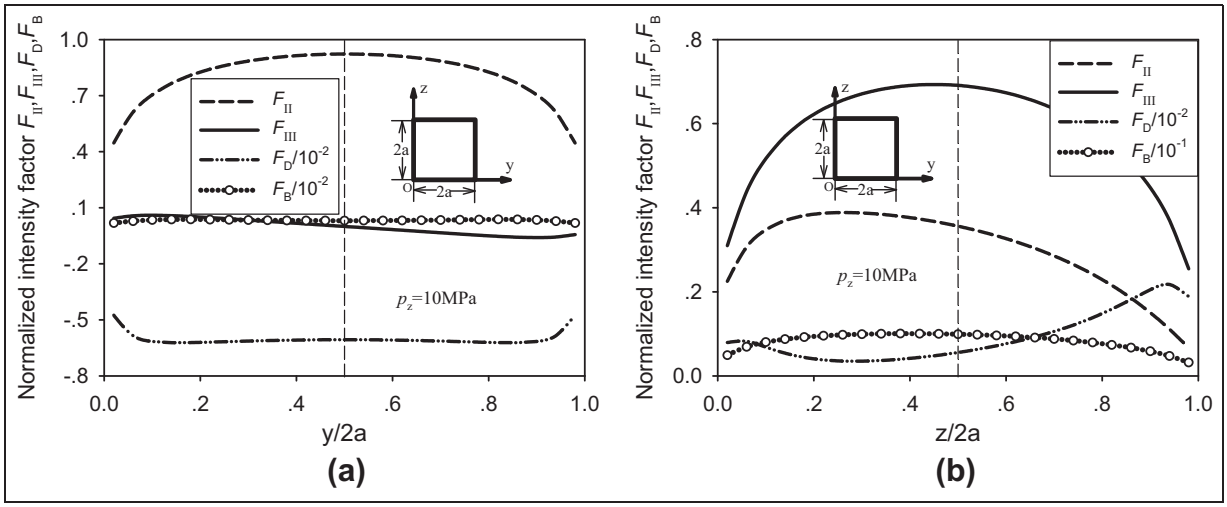

Figure 4. Variation of the normalized extended field intensity factors along the crack front parallel to (a) *y*-axis and (b) *z*-axis under mechanical load p_z = 10 MPa on the crack surface (other loads on the crack surface are zero).

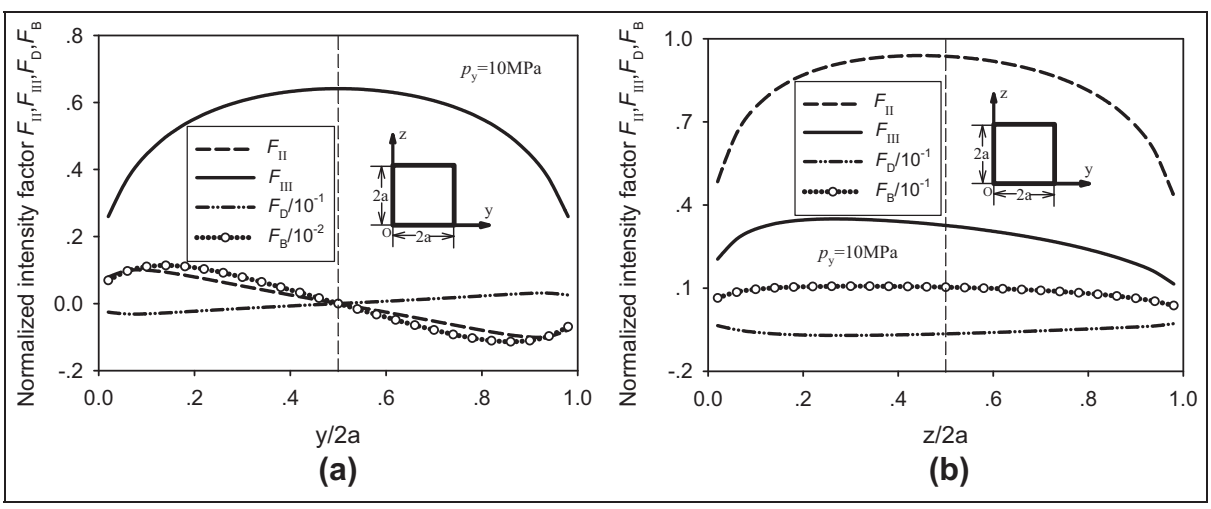

Figure 5. Variation of the normalized extended field intensity factors along the crack front parallel to (a) *y*-axis and (b) *z*-axis under mechanical load p_y = 10 MPa on the crack surface (other loads on the crack surface are zero).

no induced mode I stress intensity factor. It is observed from Figures 4 and 5 that when the crack front is parallel to the *y*-axis, the extended normalized field intensity factors F_{II}, F_{III}, F_D, and F_B are either symmetric or antisymmetric with respect to the midpoint of the crack front. Furthermore, for a fixed field intensity factor, the symmetric property changes between Figures 4(a) and 5(a). For instance, the symmetric F_{II} in Figure 4(a) becomes antisymmetric in Figure 5(a). However, along the crack front parallel to the *z*-axis (which is along the poling direction), no symmetric feature exists (Figures 4(b) and 5(b)). It is also noted that under the mechanical loading, the magnitudes of the normalized electric displacement intensity factor F_D and magnetic induction intensity factor F_B are much smaller than the mechanical factors F_{II} and F_{III}, due to the weakly coupling coefficients in the material. Moreover, under the mechanical shear load p_z, the largest intensity factor is F_{II} along the *y*-axis (Figure 4(a)) and F_{III} along the *z*-axis (Figure 4(b)), with F_{II} (Figure 4(a)) being larger than F_{III} (Figure 4(b)); however, under the shear load p_y, the largest intensity factor is F_{III} along the *y*-axis (Figure 5(a)) and F_{II} along the *z*-axis (Figure 5(b)), with also F_{II} (Figure 5(b)) being larger than F_{III} (Figure 5(a)).

Figure 6(a) and (b) shows the normalized extended field intensity factors F_{II}, F_{III}, F_D, and F_B along the crack fronts under the electric loading $\overline{D} = 0.1\,\mathrm{C/m^2}$, while the other loads are zero. These normalized intensity factors are defined as follows

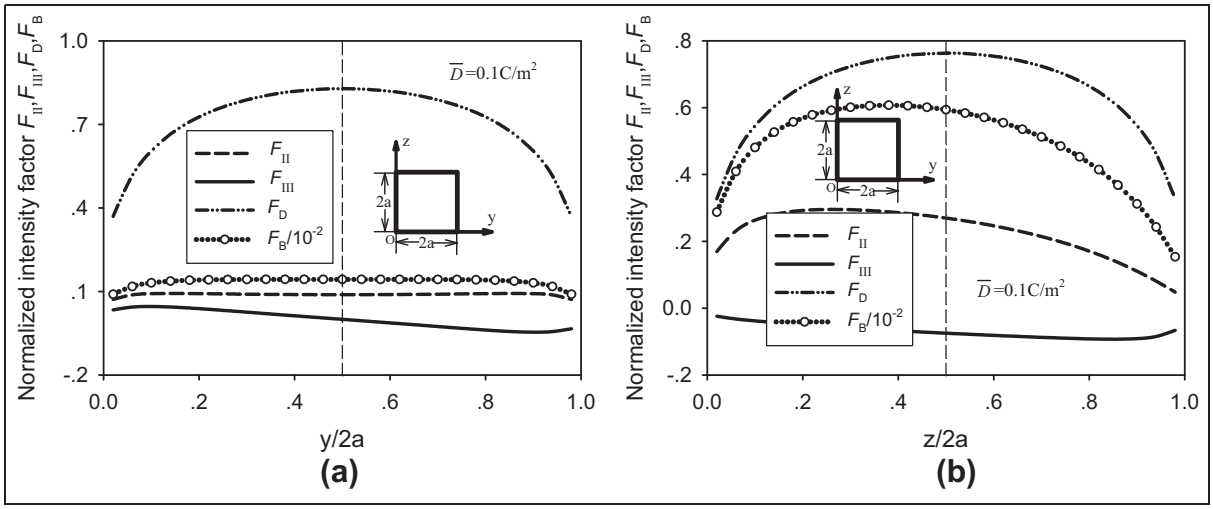

Figure 6. Variation of the normalized extended field intensity factors along the crack front parallel to (a) *y*-axis and (b) *z*-axis under electric load $\overline{D} = 0.1\ \mathrm{C/m^2}$ on the crack surface (other loads on the crack surface are zero).

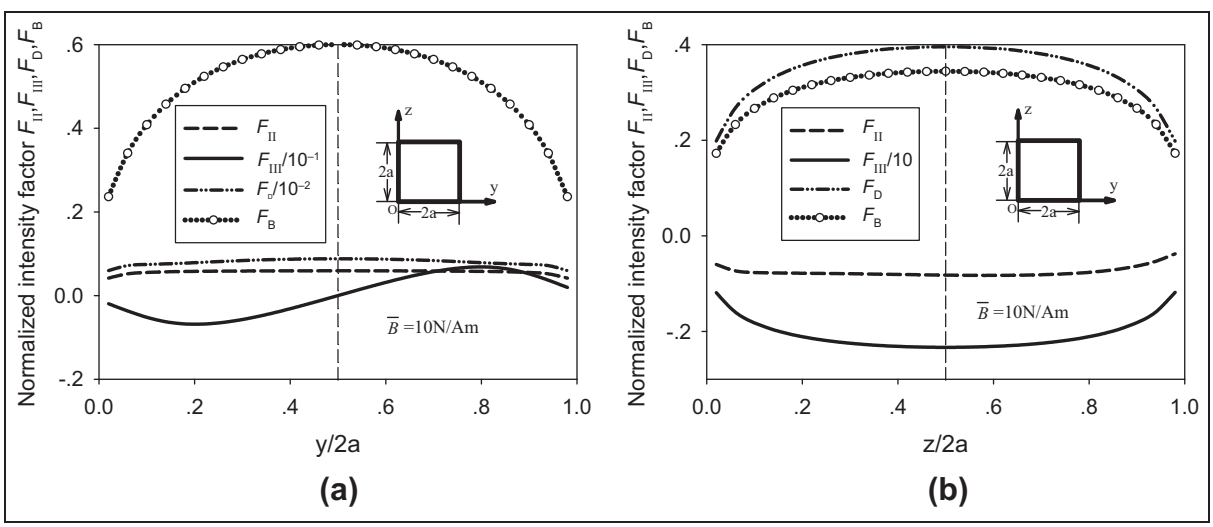

Figure 7. Variation of the normalized extended field intensity factors along the crack front parallel to (a) *y*-axis and (b) *z*-axis under magnetic load $\overline{B} = 10\ \mathrm{N/A\,m}$ on the crack surface (other loads on the crack surface are zero).

$$F_{\mathrm{II}} = \frac{\chi_1 K_{\mathrm{II}}}{\overline{D}\sqrt{\pi a}},\ F_{\mathrm{III}} = \frac{\chi_1 K_{\mathrm{III}}}{\overline{D}\sqrt{\pi a}},$$
$$F_{\mathrm{D}} = \frac{K_{\mathrm{D}}}{\overline{D}\sqrt{\pi a}},\ F_{\mathrm{B}} = \frac{K_{\mathrm{B}}}{\chi_3 \overline{D}\sqrt{\pi a}} \tag{23}$$

where $\chi_3 = \chi_2/\chi_1$. Figure 7(a) and (b) shows the corresponding factors under the magnetic loading $\overline{B} = 10\ \mathrm{N/A\,m}$, which are normalized as follows

$$F_{\mathrm{II}} = \frac{\chi_2 K_{\mathrm{II}}}{\overline{B}\sqrt{\pi a}},\ F_{\mathrm{III}} = \frac{\chi_2 K_{\mathrm{III}}}{\overline{B}\sqrt{\pi a}},$$
$$F_{\mathrm{D}} = \frac{\chi_3 K_{\mathrm{D}}}{\overline{B}\sqrt{\pi a}},\ F_{\mathrm{B}} = \frac{K_{\mathrm{B}}}{\overline{B}\sqrt{\pi a}} \tag{24}$$

First, we also observed that these intensity factors are either symmetric or antisymmetric along the crack front parallel to the *y*-axis (Figures 6(a) and 7(a)) and that this symmetry feature disappears along the crack front parallel to the *z*-axis due to the poling direction selected (Figures 6(b) and 7(b)). Figure 6 also demonstrates that the electric displacement intensity factor F_D is relatively larger than factors F_{II}, F_{III}, and F_B under the electric load $\overline{D}$. Under the magnetic load $\overline{B}$ and along the crack front parallel to the *y*-axis, the intensity factors F_{II}, F_{III}, and F_D are all very small, as compared to F_B (Figure 7(a)). However, under magnetic load $\overline{B}$ and along the *z*-axis, the intensity factors F_{III} and F_D

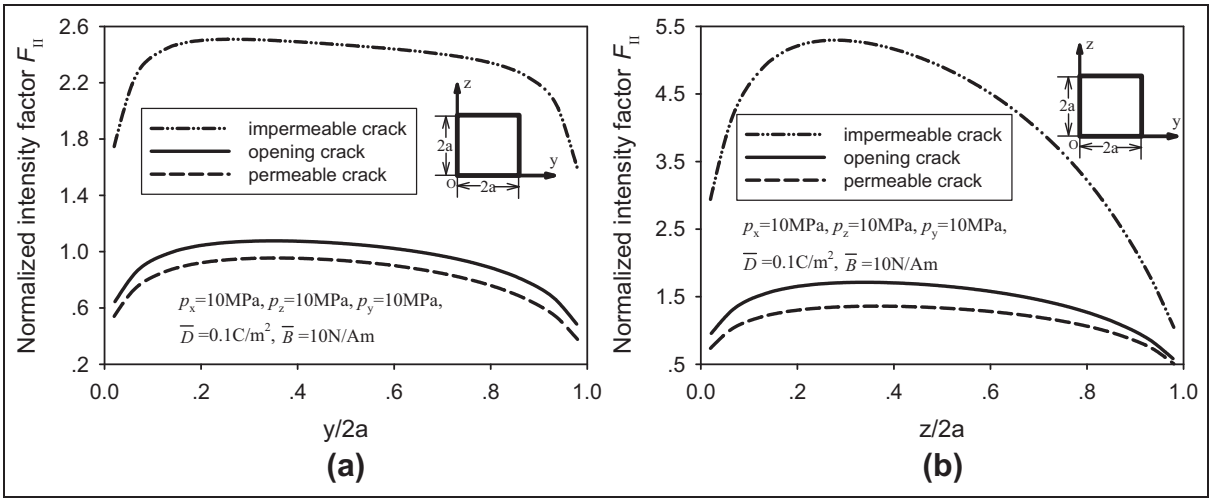

Figure 8. Normalized field intensity factor F_{II} along the crack front parallel to (a) y-axis and (b) z-axis under different electric and magnetic boundary conditions with applied loads on the crack surface as p_x = 10 MPa, p_z = 10 MPa, p_y = 10 MPa, $\overline{D} = 0.1\ \mathrm{C/m^2}$, and $\overline{B} = 10\,\mathrm{N/A}$.

are larger than the magnetic induction intensity factor F_B, an interesting feature possibly caused by the piezomagnetic and electromagnetic coupling effects.

A square crack under other electrical and magnetic conditions

We now study the effect of other electrical and magnetic boundary conditions on the field intensity factor. Besides the electrically and magnetically impermeable case (equation (5)), the electrically and magnetically permeable case (equation (6)) and the opening crack case (equation (9)) are also considered for comparison. Furthermore, on the crack face, the combined loadings p_x = 10 MPa, p_z = 10 MPa, p_y = 10 MPa, $\overline{D} = 0.1\,\mathrm{C/m^2}$, and $\overline{B} = 10\,\mathrm{N/A}$ are applied. Under these conditions, the normalized extended field intensity factors are calculated and presented in Figures 8 to 11 where the normalization is defined as

$$F_{\mathrm{II}} = \frac{K_{\mathrm{II}}}{p_y\sqrt{\pi a}}, \quad F_{\mathrm{III}} = \frac{K_{\mathrm{III}}}{p_z\sqrt{\pi a}}, \qquad F_{\mathrm{D}} = \frac{K_{\mathrm{D}}}{\overline{D}\sqrt{\pi a}}, \quad F_{\mathrm{B}} = \frac{K_{\mathrm{B}}}{\overline{B}\sqrt{\pi a}} \tag{25}$$

Figure 8(a) and (b) shows the normalized field intensity factor F_{II} along the crack fronts that are parallel to the y- and z-axes, respectively, under different crack face conditions. It is obvious that the intensity factor under the electrically and magnetically impermeable crack face condition is much larger than the ones under the permeable or opening crack face conditions. This feature does not exist in the corresponding intensity factor F_{III} shown in Figure 9(a) and (b), where this intensity factor showed an approximate antisymmetric variation along the y-axis and a much large magnitude (negative) along the z-axis. It is interesting to observe from Figures 10(a), 10(b), 11(a), and 11(b) that both the field intensity factors F_D and F_B show similar behavior along both the y-axis and z-axis even though the z-axis is the poling axis of the material. We also note that in Figures 8 to 11, the intensity factors associated with an impermeable crack have a much larger magnitude than those with either an permeable or opening crack, a feature could be useful in controlling fracture behaviors in MEE solids.

Conclusion

The extended displacement discontinuity method is proposed to study the fracture problem in a 3D transversely isotropic MEE medium weakened by vertical planar cracks. By using the Somigliana identity along with the point-displacement discontinuity Green's functions, the hyper-singular boundary integral equations for the unknown displacement discontinuities along the crack face has been derived, in which the effect of different electric and magnetic boundary conditions can be considered. The singularity features along the crack fronts are analyzed, and the extended field intensity factors are expressed in terms of the extended displacement discontinuities on the crack face. Based on the point-displacement discontinuity Green's functions, we then derive the exact closed-form fundamental solutions due to a constant displacement discontinuity over a rectangle and form the boundary element formulation. Numerical examples are finally carried out for a vertical square crack. From the solutions we derived and the numerical examples presented, we find the following interesting features.

The coupling behavior for the vertical crack case is different from most previous studies where the crack was assumed to be parallel to the isotropic plane. For

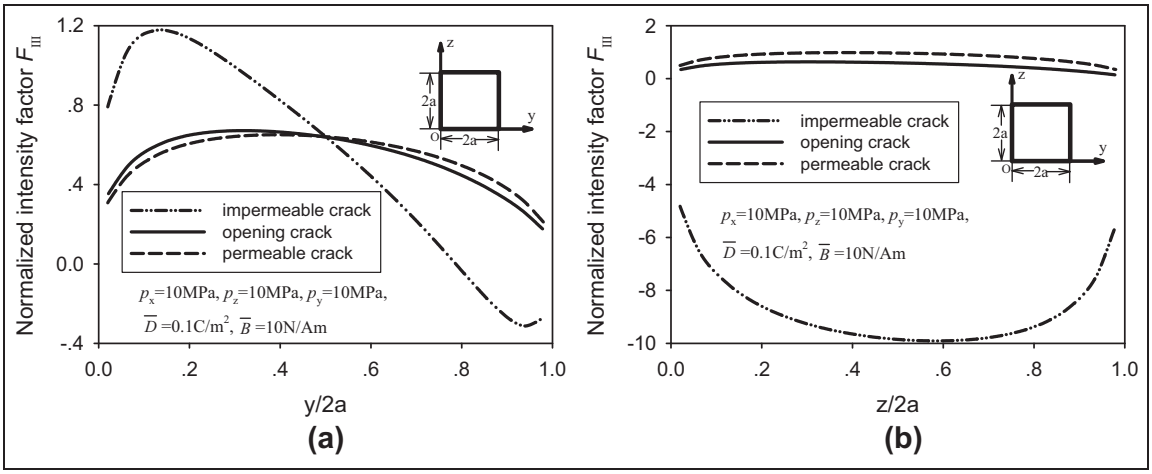

Figure 9. Normalized field intensity factor F_{III} along the crack front parallel to (a) *y*-axis and (b) *z*-axis under different electric and magnetic boundary conditions with applied loads on the crack surface as p_x = 10 MPa, p_z = 10 MPa, p_y = 10 MPa, $\overline{D}$ = 0.1 C/m^2, and $\overline{B}$ = 10 N/A.

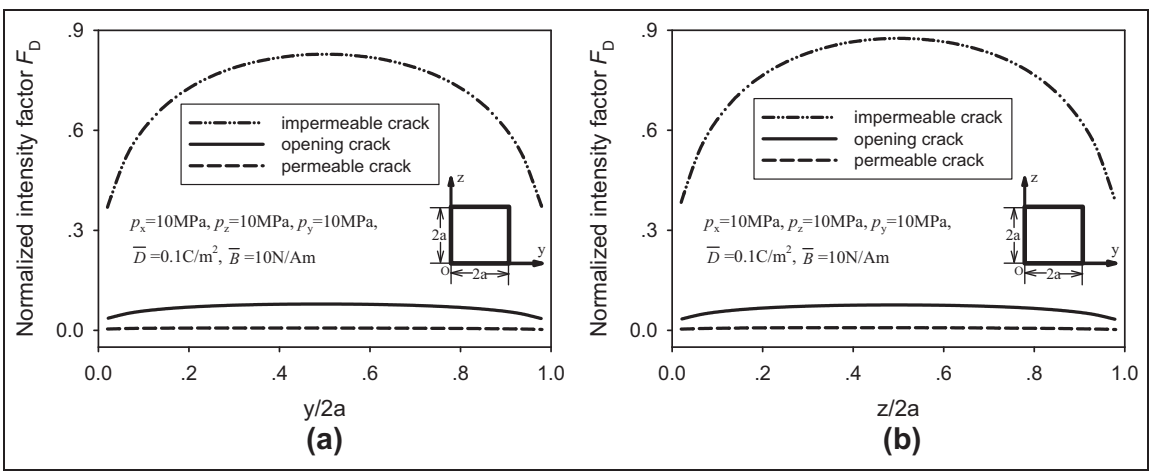

Figure 10. Normalized field intensity factor F_D along the crack front parallel to (a) *y*-axis and (b) *z*-axis under different electric and magnetic boundary conditions with applied loads on the crack surface as p_x = 10 MPa, p_z = 10 MPa, p_y = 10 MPa, $\overline{D}$ = 0.1 C/m^2, and $\overline{B}$ = 10 N/A.

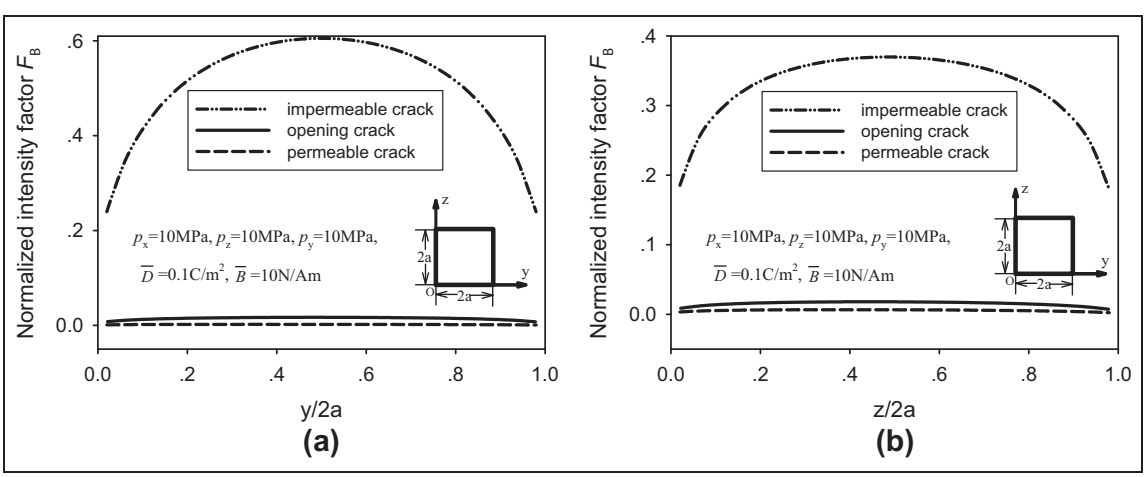

Figure 11. Normalized field intensity factor F_B along the crack front parallel to (a) *y*-axis and (b) *z*-axis under different electric and magnetic boundary conditions with applied loads on the crack surface as p_x = 10 MPa, p_z = 10 MPa, p_y = 10 MPa, $\overline{D}$ = 0.1 C/m^2, and $\overline{B}$ = 10 N/A.

the vertical crack case, the displacement discontinuity Δu_x is decoupled from the other displacement discontinuities and depends only on the normal traction p_x on the crack face, while the extended displacement discontinuities Δu_y, Δu_z, $\Delta\varphi$, and $\Delta\psi$ are all coupled together. As such, the mode I stress intensity factor depends only on the normal displacement discontinuity Δu_x, while the other field intensity factors are related to the displacement discontinuities Δu_y, Δu_z, $\Delta\varphi$, and $\Delta\psi$ due to the poling direction and crack orientation selected.

For the extended field intensity factors along the crack fronts of a vertical square crack in 3D transversely isotropic MEE space, our numerical examples showed the typical features on the variation in the intensity factors along the crack fronts (symmetric or antisymmetric along the crack front parallel to the y-axis and no symmetry variation along the crack front parallel to the z-axis). It is interesting that under a given load on the crack surface, the normalized field intensity factors along the crack front can have different magnitudes and that the maximum factor may not always be the one associated with the loading type. In particular, a magnetic load applied to the crack face could induce the mechanical and electric field intensity factors, which are larger than the induced magnetic field intensity factor. Our numerical results further demonstrate that the boundary conditions could greatly influence the extended intensity factors.

Funding

This work was supported by the National Natural Science Foundation of China (No. 11102186, No. 11072221, No. 11172273), the Program for Innovative Research Team (in Science and Technology) in the University of Henan Province (2010IRTSTHN013), and the Bairen Program in Henan Province.

References

Chen XH (2009) Dynamic crack propagation in a magneto-electro-elastic solid subjected to mixed loads: transient Mode-III problem. *International Journal of Solids and Structures* 46: 4025–4037.

Crouch SL (1976) Solution of plane elasticity problems by the displacement discontinuity method. *International Journal for Numerical Methods in Engineering* 10: 301–343.

Dinzart F and Sabar H (2012) Magnetoelectric effect in coated fibrous magnetic–piezoelectric composites. *Journal of Intelligent Material Systems and Structures* 23: 1249–1261.

Feng WJ, Su RKL, Liu JX, et al. (2010) Fracture analysis of bounded magnetoelectroelastic layer with interfacial cracks under magnetoelectromechanical loads: plane problem. *Journal of Intelligent Material Systems and Structures* 21: 581–594.

Gao CF and Noda N (2004) Thermal-induced interfacial cracking of magnetoelectroelastic materials. *International Journal of Engineering Science* 42: 1347–1360.

Gao CF, Kessler H and Balke H (2003a) Crack problems in magnetoelectroelastic solids. Part I: exact solution of a crack. *International Journal of Engineering Science* 41: 969–981.

Gao CF, Kessler H and Balke H (2003b) Crack problems in magnetoelectroelastic solids. Part II: general solution of collinear cracks. *International Journal of Engineering Science* 41: 983–994.

Huang GY, Wang BL and Mai YW (2009) Effective properties of magnetoelectroelastic materials with aligned ellipsoidal voids. *Mechanics Research Communications* 36: 563–572.

Jiang X and Pan E (2004) Exact solution for 2D polygonal inclusion problem in anisotropic magnetoelectroelastic full-, half-, and bimaterial-planes. *International Journal of Solids and Structures* 41: 4361–4382.

Lee J, Boyd JG and Lagoudas DC (2005) Effective properties of three-phase electro-magneto-elastic composites. *International Journal of Engineering Science* 43: 790–825.

Li JY and Dunn ML (1998) Micromechanics of magnetoelectroelastic composite material: average fields and effective behavior. *Journal of Intelligent Material Systems and Structures* 7: 404–416.

Li YS, Feng WJ and Xu ZH (2009) Fracture analysis of cracked 2D planar and axisymmetric problems of magneto-electro-elastic materials by the MLPG coupled with FEM. *Computer Methods in Applied Mechanics and Engineering* 198: 2347–2359.

Liu JX, Liu XG and Zhao YB (2001) Green's functions for anisotropic magnetoelectroelastic solids with an elliptical cavity or a crack. *International Journal of Engineering Science* 39: 1405–1418.

Nye JF (1957) *Physical Properties of Crystals*. Oxford: Clarendon Press.

Pan E and Yuan FG (2000) Boundary element analysis of three-dimensional cracks in anisotropic solids. *International Journal for Numerical Methods in Engineering* 48: 211–237.

Rangelov T, Stoynov Y and Dineva P (2011) Dynamic fracture behavior of functionally graded magnetoelectroelastic solids by BIEM. *International Journal of Solids and Structures* 48: 2987–2999.

Rojas-Díaz R, Denda M, García-Sánchez F, et al. (2012) Dual BEM analysis of different crack face boundary conditions in 2D magnetoelectroelastic solids. *European Journal of Mechanics A: Solids* 31: 152–162.

Rojas-Díaz R, García-Sánchez F and Sáez A (2010) Analysis of cracked magnetoelectroelastic composites under time-harmonic loading. *International Journal of Solids and Structures* 47: 71–80.

Sih GC and Song ZF (2003) Magnetic and electric poling effects associated with crack growth in $BaTiO_3$–$CoFe_2O_4$ composite. *Theoretical and Applied Fracture Mechanics* 39: 209–227.

Sih GC, Jones R and Song ZF (2003) Piezomagnetic and piezoelectric poling effects on mode I and II crack

initiation behavior of magnetoelectroelastic materials. *Theoretical and Applied Fracture Mechanics* 40: 161–186.

Sladek J, Sladek V, Solek P, et al. (2008) Fracture analysis of cracks in magneto-electro-elastic solids by the MLPG. *Computational Mechanics* 42: 697–714.

Soh AK and Liu JX (2005) On the constitutive equations of magnetoelectroelastic solids. *Journal of Intelligent Material Systems and Structures* 16: 597–602.

Spyropoulos CP, Sih GC and Song ZF (2003) Magnetoelectroelastic composite with poling parallel to plane of line crack under out-of-plane deformation. *Theoretical and Applied Fracture Mechanics* 39: 281–289.

Wang BL (2012) Fracture and effective properties of finite magnetoelectroelastic media. *Journal of Intelligent Material Systems and Structures* 23: 1699–1712.

Wünsche M, Sáez A, Zhang CZ, et al. (2012) Semi-permeable cracks in magnetoelectroelastic solids under impact loading. *Key Engineering Materials* 488–489: 751–754.

Zhao MH, Fan CY, Liu T, et al. (2007a) Extended displacement discontinuity Green's functions for three-dimensional transversely isotropic magneto-electro-elastic media and applications. *Engineering Analysis with Boundary Elements* 31: 547–558.

Zhao MH, Fan CY, Yang F, et al. (2007b) Analysis method of planar cracks of arbitrary shape in the isotropic plane of a three-dimensional transversely isotropic magnetoelectroelastic medium. *International Journal of Solids and Structures* 44: 4505–4523.

Zhao MH, Liu YJ and Cheng C (1994) Boundary-integral equations and the boundary-element method for three-dimensional fracture mechanics. *Engineering Analysis with Boundary Elements* 13: 333–338.

Zhao MH, Xu GT and Fan CY (2010) Numerical method of crack analysis in 2D finite magnetoelectroelastic media. *Computational Mechanics* 45: 401–413.

Zhao MH, Zhang RL, Fan CY, et al. (2012) Three-dimensional extended displacement discontinuity method for vertical cracks in transversely isotropic piezoelectric media. *Engineering Analysis with Boundary Elements* 36: 1406–1415.

Zhong XC (2009) Analysis of a dielectric crack in a magnetoelectroelastic layer. *International Journal of Solids and Structures* 46: 4221–4230.

Appendix 1

Unit point-displacement discontinuity Green's functions

Using the versatile method for extended displacement discontinuity Green's functions (Zhao et al., 2007a), based on the Somigliana identity and the point-force Green's functions, we derive the point-displacement discontinuity Green's functions for a discontinuity surface element vertical to the plane of isotropy in a three-dimensional (3D) transversely isotropic MEE medium.

(1) Green's functions due to a unit point-displacement discontinuity Δu_x

$$u_x = -2c_{66}T_5x\left(\frac{1}{R_5\tilde{R}_5^2}-\frac{2y^2}{R_5^2\tilde{R}_5^3}-\frac{y^2}{R_5^3\tilde{R}_5^2}\right)-x\sum_{i=1}^{4}T_i\left(\frac{\xi_i}{R_i^3}-2c_{66}\left(\frac{3}{R_i\tilde{R}_i^2}-\frac{2x^2}{R_i^2\tilde{R}_i^3}-\frac{x^2}{R_i^3\tilde{R}_i^2}\right)\right) \quad (26)$$

$$u_y = -2c_{66}T_5y\left(\frac{2x^2}{R_5^2\tilde{R}_5^3}+\frac{x^2}{R_5^3\tilde{R}_5^2}-\frac{1}{R_5\tilde{R}_5^2}\right)-y\sum_{i=1}^{4}T_i\left(\frac{\xi_i}{R_i^3}+2c_{66}\left(\frac{2x^2}{R_i^2\tilde{R}_i^3}+\frac{x^2}{R_i^3\tilde{R}_i^2}-\frac{1}{R_i\tilde{R}_i^2}\right)\right) \quad (27)$$

$$u_z = 2c_{66}\sum_{i=1}^{4}A_i\left(\frac{1}{R_i\tilde{R}_i}-\frac{x^2}{R_i^3\tilde{R}_i}-\frac{x^2}{R_i^2\tilde{R}_i^2}\right)-\sum_{i=1}^{4}\xi_iA_i\frac{z_i}{R_i^3} \quad (28)$$

$$\varphi = -2c_{66}\sum_{i=1}^{4}N_i\left(\frac{1}{R_i\tilde{R}_i}-\frac{x^2}{R_i^3\tilde{R}_i}-\frac{x^2}{R_i^2\tilde{R}_i^2}\right)+\sum_{i=1}^{4}\xi_iN_i\frac{z_i}{R_i^3} \quad (29)$$

$$\psi = -2c_{66}\sum_{i=1}^{4}C_i\left(\frac{1}{R_i\tilde{R}_i}-\frac{x^2}{R_i^3\tilde{R}_i}-\frac{x^2}{R_i^2\tilde{R}_i^2}\right)+\sum_{i=1}^{4}\xi_iC_i\frac{z_i}{R_i^3} \quad (30)$$

where

$$\begin{aligned} R_i &= \sqrt{x^2+y^2+z_i^2} \\ \tilde{R}_i &= \sqrt{x^2+y^2+z_i^2}+z_i, \quad (i=1,2,3,4,5) \end{aligned} \quad (31)$$

(2) Green's functions due to a unit point-displacement discontinuity Δu_y

$$u_x = -c_{66}T_5 y\left(\frac{1}{R_5^3} - \frac{2}{R_5\tilde{R}_5^2} + \frac{4x^2}{R_5^2\tilde{R}_5^3} + \frac{2x^2}{R_5^3\tilde{R}_5^2}\right) + 2c_{66}y\sum_{i=1}^{4} T_i\left(\frac{1}{R_i\tilde{R}_i^2} - \frac{2x^2}{R_i^2\tilde{R}_i^3} - \frac{x^2}{R_i^3\tilde{R}_i^2}\right) \tag{32}$$

$$u_y = -c_{66}T_5 x\left(\frac{1}{R_5^3} - \frac{2}{R_5\tilde{R}_5^2} + \frac{4y^2}{R_5^2\tilde{R}_5^3} + \frac{2y^2}{R_5^3\tilde{R}_5^2}\right) + 2c_{66}x\sum_{i=1}^{4} T_i\left(\frac{1}{R_i\tilde{R}_i^2} - \frac{2y^2}{R_i^2\tilde{R}_i^3} - \frac{y^2}{R_i^3\tilde{R}_i^2}\right) \tag{33}$$

$$u_z = -2c_{66}xy\sum_{i=1}^{4} A_i\left(\frac{1}{R_i^3\tilde{R}_i} + \frac{1}{{R_i}^2\tilde{R}_i^2}\right) \tag{34}$$

$$\varphi = 2c_{66}xy\sum_{i=1}^{4} N_i\left(\frac{1}{R_i^3\tilde{R}_i} + \frac{1}{{R_i}^2\tilde{R}_i^2}\right) \tag{35}$$

$$\psi = 2c_{66}xy\sum_{i=1}^{4} C_i\left(\frac{1}{R_i^3\tilde{R}_i} + \frac{1}{{R_i}^2\tilde{R}_i^2}\right) \tag{36}$$

(3) Green's functions due to a unit point-displacement discontinuity Δu_z

$$u_x = -\omega_{51}T_5\left(\frac{1}{R_5\tilde{R}_5} - \frac{y^2}{R_5^3\tilde{R}_5} - \frac{y^2}{R_5^2\tilde{R}_5^2}\right) + \sum_{i=1}^{4}\omega_{i1}T_i\left(\frac{1}{R_i\tilde{R}_i} - \frac{x^2}{R_i^3\tilde{R}_i} - \frac{x^2}{R_i^2\tilde{R}_5^2}\right) \tag{37}$$

$$u_y = -\sum_{i=1}^{5}\omega_{i1}T_i xy\left(\frac{1}{R_i^3\tilde{R}_i} + \frac{1}{R_i^2\tilde{R}_i^2}\right) \tag{38}$$

$$u_z = -x\sum_{i=1}^{4}\frac{\omega_{i1}A_i}{R_i^3} \tag{39}$$

$$\varphi = x\sum_{i=1}^{4}\frac{\omega_{i1}N_i}{R_i^3} \tag{40}$$

$$\psi = x\sum_{i=1}^{4}\frac{\omega_{i1}C_i}{R_i^3} \tag{41}$$

The Green's functions due to a unit electric potential discontinuity $\Delta\varphi$ and a unit magnetic potential discontinuity $\Delta\psi$ can be obtained simply by replacing ω_{i1} with ω_{i2} and ω_{i3}, respectively.

Making use of the constitutive equations (1), the stress, electric displacement, and magnetic induction can be calculated.

Appendix 2

Extended fundamental solutions over a rectangle

When the uniformly distributed extended displacement discontinuities Δu_{I} are applied to a rectangular element S_e of length $2a\times 2b$ in the oyz plane as shown in Figure 2, the extended fundamental solution (of the extended stresses) over the rectangle can be expressed as (only the nonzero components are listed)

$$T_{11} = 4L_{11}^5Q_1^5 + \sum_{i=1}^{4}((6L_{12}^i + 2L_{13}^i)Q_2^i - 2L_{13}^iQ_3^i - (L_{14}^i + L_{15}^i + 2L_{16}^i)Q_4^i + 3L_{15}^iQ_5^i + L_{17}^iQ_6^i) \tag{42}$$

$$\begin{aligned} &T_{22} = L_{11}^5(-4Q_1^5 + 3Q_5^5 - 2Q_4^5) - 4\sum_{i=1}^{4}L_{11}^iQ_1^i,\ T_{23} = L_{31}^5Q_9^5 - 2\sum_{i=1}^{4}L_{34}^iQ_7^i \\ &T_{24} = L_{32}^5Q_9^5 - \sum_{i=1}^{4}2L_{35}^iQ_7^i,\ T_{25} = L_{33}^5Q_9^5 - 2\sum_{i=1}^{4}L_{36}^iQ_7^i \end{aligned} \tag{43}$$

$$T_{32} = L_{21}^5(2Q_7^5 - Q_8^5) - 2\sum_{i=1}^{4} L_{21}^i Q_7^i,\ T_{33} = L_{41}^5(Q_4^5 - 3Q_5^5) - \sum_{i=1}^{4} L_{51}^i Q_4^i$$
$$T_{34} = L_{61}^5(Q_4^5 - 3Q_5^5) - \sum_{i=1}^{4} L_{71}^i Q_4^i,\ T_{35} = L_{81}^5(Q_4^5 - 3Q_5^5) - \sum_{i=1}^{4} L_{91}^i Q_4^i \tag{44}$$

$$T_{42} = L_{22}^5(2Q_7^5 - Q_8^5) - 2\sum_{i=1}^{4} L_{22}^i Q_7^i,\ T_{43} = L_{42}^5(Q_4^5 - 3Q_5^5) - \sum_{i=1}^{4} L_{52}^i Q_4^i$$
$$T_{44} = L_{62}^5(Q_4^5 - 3Q_5^5) - \sum_{i=1}^{4} L_{72}^i Q_4^i,\ T_{45} = L_{82}^5(Q_4^5 - 3Q_5^5) - \sum_{i=1}^{4} L_{92}^i Q_4^i \tag{45}$$

$$T_{52} = L_{23}^5(2Q_7^5 - Q_8^5) - 2\sum_{i=1}^{4} L_{23}^i Q_7^i,\ T_{53} = L_{43}^5(Q_4^5 - 3Q_5^5) - \sum_{i=1}^{4} L_{53}^i Q_4^i$$
$$T_{54} = L_{63}^5(Q_4^5 - 3Q_5^5) - \sum_{i=1}^{4} L_{73}^i Q_4^i,\ T_{55} = L_{83}^5(Q_4^5 - 3Q_5^5) - \sum_{i=1}^{4} L_{93}^i Q_4^i \tag{46}$$

where the functions are given as follows

$$\begin{aligned}
Q_1^i &= F_{11}^i + F_{12}^i + M_{11}^i G_{11}^i + M_{12}^i G_{12}^i - M_{13}^i G_{13}^i - M_{14}^i G_{14}^i \\
Q_2^i &= -(M_{11}^i)^3 G_{21}^i - (M_{12}^i)^3 G_{22}^i - (M_{13}^i)^3 G_{23}^i - (M_{14}^i)^3 G_{24}^i - F_{21}^i - F_{22}^i + F_{23}^i + F_{24}^i \\
Q_3^i &= M_{11}^i(-G_{31}^i + \frac{4}{3}G_{11}^i) - M_{12}^i(G_{32}^i - \frac{4}{3}G_{12}^i) - M_{13}^i(G_{33}^i + \frac{4}{3}G_{13}^i) \\
&\quad + M_{14}^i(-G_{34}^i - \frac{4}{3}G_{14}^i) + \frac{4}{3}F_{11}^i + \frac{4}{3}F_{12}^i
\end{aligned} \tag{47}$$

$$\begin{aligned}
Q_4^i &= 3(-\mathrm{M}_{11}^i G_{31}^i - \mathrm{M}_{12}^i G_{32}^i - \mathrm{M}_{13}^i G_{33}^i - \mathrm{M}_{14}^i G_{34}^i) \\
Q_5^i &= \mathrm{M}_{21}^i \mathrm{M}_{31}^i G_{31}^i + \mathrm{M}_{22}^i \mathrm{M}_{32}^i G_{32}^i + \mathrm{M}_{23}^i \mathrm{M}_{33}^i G_{33}^i + \mathrm{M}_{24}^i \mathrm{M}_{34}^i G_{34}^i \\
Q_6^i &= -(\mathrm{F}_{31}^i M_{31}^i + \mathrm{F}_{32}^i M_{32}^i + \mathrm{F}_{33}^i M_{33}^i + \mathrm{F}_{34}^i M_{34}^i)
\end{aligned} \tag{48}$$

$$\begin{aligned}
Q_7^i &= F_{41}^i + M_{41}^i(M_{11}^i - M_{13}^i) + M_{42}^i(-M_{12}^i + M_{14}^i) \\
Q_8^i &= F_{51}^i M_{12}^i + F_{52}^i M_{13}^i + F_{61}^i M_{31}^i + F_{62}^i M_{34}^i + G_{41}^i - G_{42}^i + G_{43}^i - G_{44}^i \\
Q_9^i &= \frac{1}{2}(-G_{41}^i + G_{42}^i - G_{43}^i + G_{44}^i) - M_{51}^i + M_{52}^i + M_{53}^i - M_{54}^i
\end{aligned} \tag{49}$$

with F_{kl}^i, G_{kl}^i, and M_{kl}^i being the fundamental functions, given as

$$\begin{aligned}
F_{11}^i &= \frac{4as_i z}{(b-y)^3},\ F_{12}^i = \frac{4as_i z}{(b+y)^3} \\
G_{11}^i &= \frac{(-a+z)}{(b-y)^3},\ G_{12}^i = \frac{(-a+z)}{(b+y)^3},\ G_{13}^i = \frac{(a+z)}{(b-y)^3},\ G_{14}^i = \frac{(a+z)}{(b+y)^3} \\
M_{11}^i &= \sqrt{s_i^2(a-z)^2 + (b-y)^2},\ M_{12}^i = \sqrt{s_i^2(a-z)^2 + (b+y)^2} \\
M_{13}^i &= \sqrt{s_i^2(a+z)^2 + (b-y)^2},\ M_{14}^i = \sqrt{s_i^2(a+z)^2 + (b+y)^2}
\end{aligned} \tag{50}$$

$$\begin{aligned}
F_{21}^{\mathrm{i}} &= \frac{s_i(a-z)^2}{3(b-y)^3},\ F_{22}^{\mathrm{i}} = \frac{s_i(a-z)^2}{3(b+y)^3},\ F_{23}^{\mathrm{i}} = \frac{s_i(a+z)^2}{3(b-y)^3},\ F_{24}^{\mathrm{i}} = \frac{s_i(a+z)^2}{3(b+y)^3} \\
G_{21}^{\mathrm{i}} &= \frac{1}{3s_i^2(b-y)^3(a-z)},\ G_{22}^{\mathrm{i}} = \frac{1}{3s_i^2(b+y)^3(a-z)} \\
G_{23}^{\mathrm{i}} &= \frac{1}{3s_i^2(b-y)^3(a+z)},\ G_{24}^{\mathrm{i}} = \frac{1}{3s_i^2(b+y)^3(a+z)} \\
M_{21}^{\mathrm{i}} &= -2s_i^2(a-z)^2 - (b-y)^2,\ M_{22}^{\mathrm{i}} = -2s_i^2(a-z)^2 - (b+y)^2 \\
M_{23}^{\mathrm{i}} &= -2s_i^2(a+z)^2 - (b-y)^2,\ M_{24}^{\mathrm{i}} = -2s_i^2(a+z)^2 - (b+y)^2
\end{aligned} \tag{51}$$

$$
\begin{aligned}
F_{31}^{\mathrm{i}} &= \frac{b-y}{s_i^2(a-z)},\ F_{32}^{\mathrm{i}} = \frac{b+y}{s_i^2(a-z)},\ F_{33}^{\mathrm{i}} = \frac{b-y}{s_i^2(a+z)},\ F_{34}^{\mathrm{i}} = \frac{b+y}{s_i^2(a+z)} \\
G_{31}^{\mathrm{i}} &= \frac{1}{3s_i^2(b-y)(a-z)},\ G_{32}^{\mathrm{i}} = \frac{1}{3s_i^2(b+y)(a-z)} \\
G_{33}^{\mathrm{i}} &= \frac{1}{3s_i^2(b-y)(a+z)},\ G_{34}^{\mathrm{i}} = \frac{1}{3s_i^2(b+y)(a+z)} \\
M_{31}^{\mathrm{i}} &= \frac{1}{\sqrt{s_i^2(a-z)^2+(b-y)^2}},\ M_{32}^{\mathrm{i}} = \frac{1}{\sqrt{s_i^2(a-z)^2+(b+y)^2}} \\
M_{33}^{\mathrm{i}} &= \frac{1}{\sqrt{s_i^2(a+z)^2+(b-y)^2}},\ M_{34}^{\mathrm{i}} = \frac{1}{\sqrt{s_i^2(a+z)^2+(b+y)^2}}
\end{aligned}
\tag{52}
$$

$$
\begin{aligned}
F_{41}^{i} &= \frac{8aby}{(b-y)^2(b+y)^2}, \\
G_{41}^{\mathrm{i}} &= \frac{4(a-z)}{(b-y)^2},\ G_{42}^{\mathrm{i}} = \frac{4(a-z)}{(b+y)^2},\ G_{43}^{\mathrm{i}} = \frac{4(a+z)}{(b-y)^2},\ G_{44}^{\mathrm{i}} = \frac{4(a+z)}{(b+y)^2} \\
M_{41}^{i} &= \frac{1}{s_i(b-y)^2},\ M_{42}^{i} = \frac{1}{s_i(b+y)^2}
\end{aligned}
\tag{53}
$$

$$
\begin{aligned}
F_{51}^{i} &= \frac{1}{s_i(b+y)^2}\left(-4+\frac{(b+y)^2}{(b+y)^2+s_i^2(a-z)^2}\right),\ F_{52}^{i} = \frac{1}{s_i(b-y)^2}\left(-4+\frac{(b-y)^2}{(b-y)^2+s_i^2(a+z)^2}\right) \\
M_{51}^{i} &= \frac{(b-y)^2+2s_i^2(a-z)^2}{s_i(b-y)^2\sqrt{s_i^2(a-z)^2+(b-y)^2}},\ M_{52}^{i} = \frac{(b+y)^2+2s_i^2(a-z)^2}{s_i(b+y)^2\sqrt{s_i^2(a-z)^2+(b+y)^2}} \\
M_{53}^{i} &= \frac{(b-y)^2+2s_i^2(a+z)^2}{s_i(b-y)^2\sqrt{s_i^2(a+z)^2+(b-y)^2}},\ M_{54}^{i} = \frac{(b+y)^2+2s_i^2(a+z)^2}{s_i(b+y)^2\sqrt{s_i^2(a+z)^2+(b+y)^2}}
\end{aligned}
\tag{54}
$$

$$
F_{61}^{i} = \frac{3(b-y)^2+4s_i^2(a-z)^2}{s_i(b-y)^2},\ F_{62}^{i} = \frac{3(b+y)^2+4s_i^2(a+z)^2}{s_i(b+y)^2}
\tag{55}
$$